Facile fabrication of electrochemical ZnO nanowire glucose biosensor using roll to roll printing technique

C.M. Fung[a], J.S. Lloyd[a], S. Samavat[a], D. Deganello[b] and K.S. Teng[a*]

[a] College of Engineering, Swansea University, Bay Campus, Fabian Way, Crymlyn Burrows, Swansea SA1 8EN, United Kingdom

[b] Welsh Centre for Printing and Coating, College of Engineering, Swansea University, Bay Campus, Fabian Way, Crymlyn Burrows, Swansea SA1 8EN, United Kingdom

**Corresponding Author: k.s.teng@swansea.ac.uk*

Abstract – A three electrode electrochemical enzymatic biosensor consisting of ZnO nanowires was successfully fabricated using flexographic printing technique. The incorporation of ZnO nanowires at the working electrode provides advantages such as simple functionalization and high surface area for enhanced sensitivity. The flexographic printing technique allows ultra-high throughput and low cost mass production of devices due to the roll-to-roll nature of the technique. Therefore, the techniques developed here are prudent to the development of technologies capable of meeting the vast market demand for biosensing. Carbon electrodes, silver/silver chloride reference electrodes and ZnO seed layer precursors were directly printed onto a flexible plastic substrate through flexographic printing. The printing process was optimised to allow a suitable seed layer to be formed on the porous printed-carbon electrode to allow selective growth of ZnO nanowires using a hydrothermal growth method. The ZnO nanowires were subsequently functionalised with glucose oxidase, which was used in this work to form a glucose sensor as an exemplary use of the device. The fabricated nanowire electrochemical biosensing devices showed a typical sensitivity of 1.2 ± 0.2 μA mM^{-1} cm^{-2} with a linear response to the addition of glucose over a concentration range of 0.1 mM to 3.6 mM.

Keywords: flexographic, printing, biosensor, electrochemical, zinc oxide, nanowires

1. Introduction

Since the early work on zinc oxide (ZnO) nanostructures, they have been investigated for a variety of applications ranging from photonics to sensing. Numerous investigations have been carried out using ZnO nanostructures for different types of sensors, such as gas sensors [1,2] and biosensors [3–7], due to their advantageous electrical, chemical and optical properties. ZnO nanostructures are well-known for ease of immobilizing various enzymes such as glucose oxidase (GOx) for the detection of glucose. This is partly due to the high isoelectric point (IEP) of the ZnO nanostructures, which is around 9.5 [8]. At physiologically relevant pH values of around pH 7.5, this high IEP of the ZnO nanostructures, provides a positively charged surface. This is particularly useful for the simple electrostatic immobilisation of enzymes, such as GOx, having a low IEP of approximately 4.2 [9] which have a net negative charge at physiological pH [10]. ZnO nanostructures also have other advantages, for example, their high surface to volume ratio results in improved sensitivity. Also, their biocompatibility and non-toxicity allows the enzyme to retain activity while immobilised on the surface [11,12]. This combination of properties makes ZnO nanowires particularly valuable candidates for biosensing applications.

Enzymatic biosensors based on the use of ZnO nanowires have been reported by others for the detection of biomarkers such as glucose [11,13] and Urea [14]. Previous studies on ZnO mostly focus on ZnO nanowires grown on a conducting substrate, which forms only a working electrode. These working electrodes tend to be evaluated with the use of off-chip, commercially-available, silver/silver chloride (Ag/AgCl) reference electrodes and a piece of metal wire (or equivalent) as a counter electrode to form a three electrode electrochemical sensing setup. ZnO biosensing devices, incorporating multiple electrodes have been demonstrated for electrochemical impedance spectroscopy detection [15]. For these devices, a two electrode system is adopted and the fabrication process covers both electrodes with the ZnO material. However, for the fabrication of three electrode enzymatic biosensors the electrodes are fabricated through separate processes but on the same chip. The fabrication of such devices is challenging because the process of fabricating ZnO nanowires tends to damage Ag/AgCl reference electrodes due to the elevated growth temperature and the chlorination of Ag to form a reference electrode tends to damage ZnO nanowires. Therefore, the fabrication of separate working, counter and reference electrodes selectively patterned onto a substrate presents a challenge. Generally, patterning of ZnO layers is carried out using photolithographic techniques [9,16–18] and laser patterning [19,20] . However, these techniques require cleanroom facilities and expensive high vacuum equipment or sophisticated laser setups. This means that the production of devices

incorporating ZnO nanowires would suffer from high setup costs and relatively low throughput in production, thus resulting in high product costs. Printing techniques can provide high throughput fabrication of devices as it has the ability to selectively pattern materials directly onto substrates. Several printing techniques have been used in the past to achieve selective patterning of materials during device fabrication, such as screen printing [21], inkjet printing [22,23] and flexographic printing. Of these methods, flexographic printing benefits from continuous roll-to-roll high-speed printing, hence most suitable for high volume production. Previously, Kempa *et al.* reported applying flexographic printing to the fabrication of ring oscillators [24]. In addition to electronic device fabrication, Fischer *et al.* and Baker *et al.* reported flexographic printing of carbon nanotubes [25] and graphene nanoplatelets [26] respectively. The authors have previously demonstrated the use of flexographic printing for the direct deposition of gold nanoparticles [27] and the selective patterning of seed layers for the hydrothermal synthesis of ZnO nanowires [28]. More recently, the authors have also demonstrated the creation of nanotextured surfaces on flexographic printed ZnO thin films [29].

This article reports the novel use of flexographic printing techniques for the fabrication of ZnO nanowire electrochemical biosensors. The fabrication technique is capable of mass producing such devices at relatively low cost and thus making them commercially viable. An electrochemical sensor is fabricated using flexographic printing to selectively pattern the substrate with the three electrodes (i.e. working, counter and reference electrodes) and subsequently to selectively pattern a ZnO seed layer onto the carbon working electrode. This allows the subsequent hydrothermal synthesis of ZnO nanowires, only at the desired area of the device. Carbon was used as the conductive material for the counter and working electrodes in this work. Carbon inks are widely used in biosensor applications due to the excellent electrochemical properties and stability of the material. After a simple functionalization procedure the biosensor is demonstrated for the detection of glucose, as an exemplar biomarker. Other biomarkers could be detected by using an appropriate surface functionalization on the ZnO nanowires.

2. Experimental Details

2.1 Materials

The biosensors were fabricated on polyimide substrates of 0.15 mm in thickness which was purchased from Lohmann Technologies UK Ltd (Milton Keynes, UK). Isopropanol (IPA), 10 mM phosphate buffer saline (PBS) solution with pH 7.4, Sodium Chloride (NaCl) and D-glucose anhydrous were purchased from Fisher Scientific

(Leicestershire, UK). Zinc acetate dihydrate and Hexamethylenetetramine were purchased from Sigma Aldrich (Dorset, UK). The conductive inks, such as Ag/AgCl (C2040308D2) and carbon (C2080529P7), were purchased from Gwent (Pontypool, UK). Glucose oxidase (GOx), 259 U/mg, was purchased from BBI Solutions (Cardiff, UK). All chemicals used were of analytical grade and used without further purification unless otherwise stated.

2.2 Biosensor fabrication overview

This article presents a simple fabrication process that is suitable for high volume production of nanowire biosensors at relatively low cost using flexographic printing technique. Figure 1(a) shows a 3D representation of the IGT Reprotest Printability Tester F1 Flexographic Printer used for this work and the printing sequence for the fabrication of the biosensor. The first step was to print the Ag/AgCl reference electrode as shown in Figure 1(b). The carbon counter and working electrodes were subsequently printed, as shown in Figure 1(c). Figure 1(d) shows the precursor ink for the seed layer, patterned onto the working electrode at the sensing area, via the same printing technique. After annealing the samples, nanowires were synthesised from the printed seed layer through a hydrothermal growth process. Three electrical wires were attached to the connection pads of the as-grown sample with conductive glue for connection to the potentiostat and the sample was then masked with photoresist or paraffin wax. This masking leaves just the sensing area and the connection pads exposed, as shown in Figure 1(e). The device was then functionalised with GOx and subsequently tested for the detection of glucose. Figure 1(f) shows an optical image of a printed device before masking. The area of nanowire growth can be seen in the upper right portion of the working electrode (marked with *).

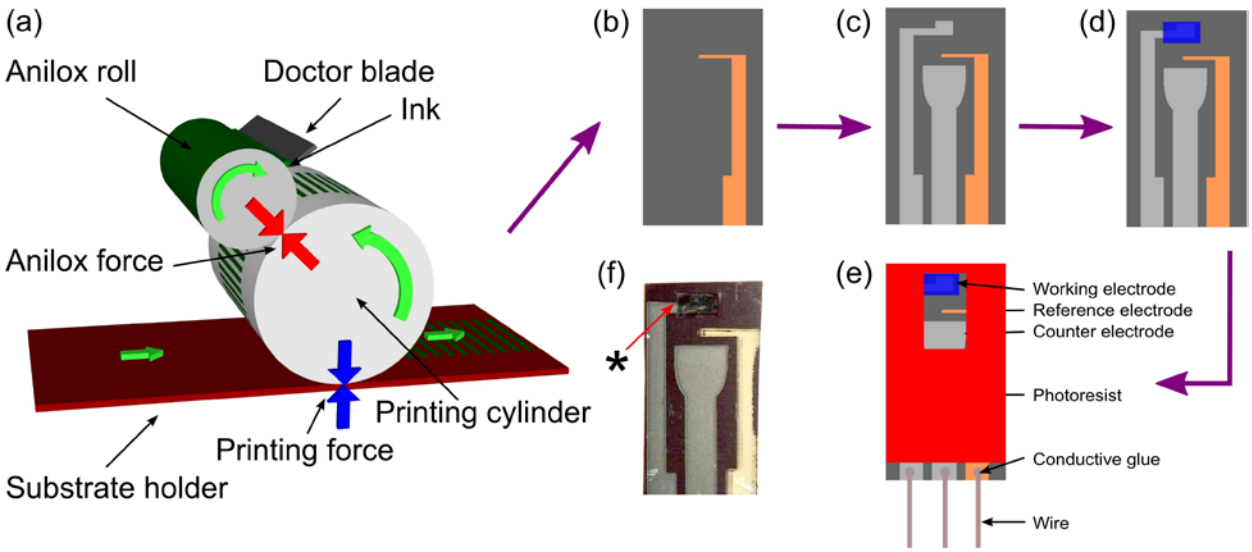

Figure 1: Flow diagram of the printing process with (a) showing a 3D representation of the flexographic printer, (b) printed Ag/AgCl electrode, (c) printed carbon electrodes, (d) printed zinc acetate precursor, (e) masked device and (f) an optical image of a device before masking (* shows area of nanowire growth, the location of SEM images shown in figure 2).

2.3 Printing conductive electrodes and zinc acetate precursor

During flexographic printing, ink was placed on the ceramic anilox roller as shown in Figure 1(a). The surface of the anilox roller consisted of numerous finely engraved cells. The doctor blade served to remove excess ink from the anilox and the flow of ink was controlled by the volume of the engraved cells. Contact between the anilox roller and the printing plate caused ink transfer onto the printing plate. The printing plate, which was patterned with a relief of the desired design, then made contact with the polyimide substrate transferring ink in the relief pattern. There were several parameters, defined below in Table 1, which required optimisation for each ink, to achieve the desired results.

The three inks used in this work were the commercially available Ag/AgCl ink used to produce a suitable reference electrode, a commercially available carbon ink for the working and counter electrodes and a zinc acetate precursor ink to form a seed layer for the growth of ZnO nanowires. The formulation of this precursor ink was 1.0975 g of zinc acetate in 10 ml deionised water and 40 ml IPA.

After printing the Ag/AgCl and carbon inks, the sample was heated in the oven at 150°C for 10 minutes to allow curing of the inks. The zinc acetate precursor ink also required heating after printing in order to achieve

decomposition of zinc acetate to form ZnO nanocrystals, which acted as seeds for the growth of the ZnO nanowires. Previously, different temperatures have been used for the decomposition of zinc acetate to form nanocrystalline ZnO seed layers. Plakhova *et al.* investigated the decomposition of zinc acetate at different temperatures and suggested that a decomposition temperature of 350^{o}C was required for complete decomposition to ZnO [30]. However, such high temperatures would damage the printed Ag/AgCl electrode. A lower annealing temperature was therefore highly desirable and would also allow the use of low-cost organic substrates. Annealing temperatures of 150°C or even 100°C were used to obtain sufficient decomposition of zinc acetate to achieve dense and uniform nanowire growth as demonstrated by Wahid *et al.* [31]. Here, it was found that annealing the printed zinc acetate precursor at 150^{o}C for 30 minutes was sufficient to form a seed layer which enabled dense and uniform ZnO nanowire growth. In addition to the thermal annealing method, the authors [32] have previously reported the use of ultraviolet light for photodecomposition of the zinc acetate to form a seed layer with the potential to reduce the decomposition time to seconds. Such photodecomposition technique can be easily incorporated into a flexographic printing press.

2.4 Synthesis of ZnO nanowires

ZnO nanowires were synthesised using hydrothermal growth method in an aqueous solution of 10 mM zinc acetate dihydrate and 10 mM Hexamethylenetetramine which was thoroughly mixed for 10 minutes prior to use. The prepared growth solution was poured into an open 250 ml beaker and placed in the water bath at 70°C and left to heat for 30 minutes. Another beaker was filled with deionised water and placed in the water bath at the same time. After 30 minutes, the sample was immersed into the deionised water for 5 to 10 seconds in order to warm the substrate. The sample was then immediately transferred to the growth solution where it was floated on the solution surface and left for around 6 hours in order to allow ZnO nanowires to grow from the seed layer. The preheating of the sample improved the selectivity of the resultant growth. It was found that nanowire growth onto a substrate added directly to the growth solution occasionally resulted in nanowire growth outside of the printed seed layer region. This unwanted nanowire growth was thought to be caused by condensation of the growth solution onto the cold substrate on insertion to the solution allowing some self-seeding to take place. The temperature of the growth solution and the duration of the growth could be varied to control the length and diameter of the ZnO nanowires [33].

2.5 Sensor preparation and functionalization

Electrical wires were attached to the sample and photoresist was applied around the sensing area leaving the three electrodes exposed and isolating the conductive connection tracks from the test solution. This process resulted in an exposed window of around 6 mm x 15 mm as shown in Figure 1(e). To functionalise the nanowires at the working electrode, 10 µl of GOx (7.3 mg/ml) was drop-cast onto the exposed region of the working electrode and the samples were kept overnight at 4^{o}C. Subsequently, the sample was rinsed with PBS to remove any loosely bound GOx. A schematic drawing of the sample after preparation is shown in Figure 1(e).

2.6 Characterization of ZnO nanowire device

The morphology and structure of as-grown ZnO nanowires were investigated using a Hitachi S-4800 scanning electron microscope (SEM). The SEM was equipped with an energy-dispersive x-ray (EDX) detector from Oxford Instruments providing elemental composition analysis of the grown samples. All SEM and EDX results presented here were obtained at 10kV with a working distance of between 10 mm and 13 mm. In order to evaluate the crystallinity of the as grown ZnO nanowires, a Bruker D8 Discover x-ray diffraction (XRD) system, equipped with a Cu_Kα x-ray source and a Lynxeye detector was employed. Stability tests for the printed Ag/AgCl reference electrode and glucose sensing properties of the final devices were carried out using a CompactStat (Ivium Technologies) potentiostat.

3. Results and discussion

3.1 Device fabrication

As described above, the fabrication of the device was initiated by the printing of Ag/AgCl ink to provide the reference electrode and carbon ink for the conductive working and counter electrodes. The carbon working electrode was then selectively overprinted with the precursor ink to form a seed layer for the selective growth of ZnO nanowires. The ZnO nanowires were functionalized and finally the electrochemical properties of the device were evaluated. For the printing process, several printing parameters were optimised to enable high quality printing. The optimised parameters, for the printing of the different inks used in this work, are presented in Table 1. The printing parameters for Ag/AgCl and carbon inks were optimised to produce low density of pinholes and good conductivity of the printed inks on the substrate. As for the seed layer, the optimisation was to ensure dense and uniform coverage of ZnO nanowires were grown over the working electrode.

	Anilox volume (cm^3m^{-2})	Anilox force (N)	Printing force (N)	Printing speed (m/s)
Carbon	12	150	150	0.6
Ag/AgCl	24	150	100	0.4
Zinc acetate precursor ink	12	125	150	0.2

Table 1: Optimised printing parameters for the different inks.

SEM images of the fabricated ZnO nanowire device, using the optimized printing parameters, are shown in Figure 2. The image shows the intersection between the polyimide substrate (left side of image) and printed carbon working electrode (right side of image). The location of the intersection is indicated in Figure 1(f) by an *. The image shows an area of printed seed layer (top of image), which after growth of the ZnO nanowires, becomes clearly visible showing uniform growth over the polyimide and carbon ink surfaces. Figure 2 also shows an area of no seed layer, at the bottom of the image, where there was no nanowire growth on either the carbon electrode or polyimide due to the absence of a seed layer. The polyimide in the bottom left of the image experienced charging under the SEM due to the poor conductivity of the substrate. The top left of the image (polyimide with seed layer) shows little charging due to the ZnO nanowire coverage. The left and right insets, shown at the top of Figure 2, show higher magnification images of the ZnO nanowire growth on the polyimide and printed carbon electrode respectively. It can be seen that dense and uniform growth of high aspect ratio ZnO nanowires was achieved over the printed carbon working electrode and polyimide surfaces. As shown in the image, the coverage of ZnO nanowires was highly uniform over the selected area where the precursor for the seed layer had been patterned using flexographic printing, despite the porosity of the underlying printed carbon electrode. A schematic drawing of the fabricated sensor is shown in Figure 1(e) with a photograph of the printed device shown in Figure 1(f). It can be seen from these figures that the printed sensor design was successfully replicated via flexographic printing.

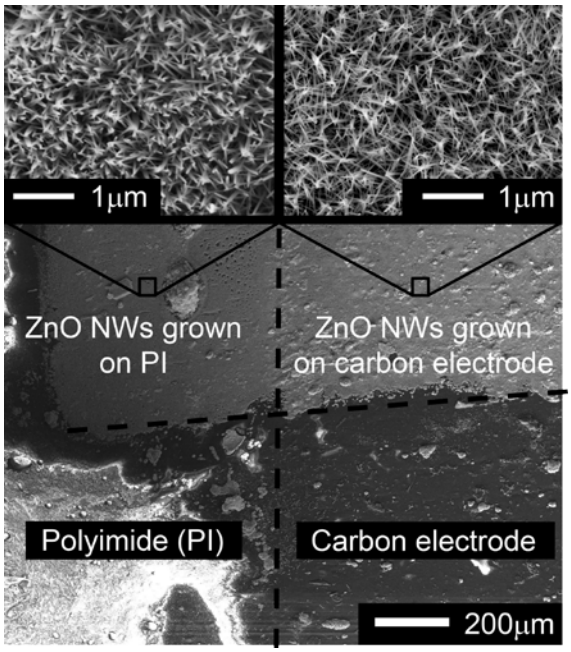

Figure 2: SEM overview of sensor at the intersection (marked with * in Figure 1f) between printed carbon electrode (right) and polyimide (left). Uniform and selective growth is observed in the printed seed region (upper portion) with inserts showing higher magnification images in the ZnO nanowires.

Flexographic printing of the carbon electrodes and the Ag/AgCl reference electrode was relatively straightforward. However, after initial prints of the seed layer precursor ink and subsequent growth of the ZnO nanowires, it was found that nanowire growth on the carbon ink was inhibited. ZnO nanowires were grown on the seed layer printed directly onto the substrate, next to the printed carbon electrode, but not on the carbon electrode itself. It is vital that the nanowire growth occurs on the carbon electrode. The absence of growth before optimisation can be seen in SEM images in the supporting information Figure S1. It can be seen from the insert in Figure S1, a high magnification SEM image of the nanowires next to the printed carbon electrode area, that the growth was dense and uniform. However, only small random patches of nanowire growth were observed in the printed carbon electrode area. The growth in the smooth substrate region occurred for a wider range of printing parameters than that on the carbon electrode. A higher volume of zinc acetate precursor ink was required in order to obtain good growth over the carbon electrode surface. This was achieved by increasing the anilox volume from 8 $cm^3 m^{-2}$ used for initial prints to 12 $cm^3 m^{-2}$. This was most likely due to the high porosity and surface roughness of the printed carbon electrode as compared to the substrate. Zinc acetate precursor ink was able to leave the surface and moved into the highly porous

carbon layer, resulting in less exposed seed layer for growth. Porosity and high surface roughness also led to a higher surface area, which naturally required more ink to coat. The uniformity of the resultant growth on the carbon electrode was also found to be improved with the use of a higher printing force so that the rougher surface of the printed carbon was more uniformly coated in precursor ink from the printing plate.

To assess the quality of the as-grown ZnO nanowires, SEM and EDX characterisations were carried out on the ZnO nanowire growth within the seeded region of the carbon working electrode. High density and uniform growth in the seeded region was observed as shown in the SEM image of figure 3(a) and the higher magnification image shown in Figure 3(b). The diameter of the nanowires was measured with the SEM to be between 30 nm and 50 nm. Figure 3(c) shows a cross-sectional image of ZnO nanowires grown on the printed seed layer on a silicon substrate. The silicon substrate was used to allow cleaving so that the length of the nanowires could be measured. Imaging from top down the two samples (ZnO nanowires on polyimide and silicon) were indistinguishable, indicating that the change in substrate had a little effect on the growth. The length of the ZnO nanowires was measured to be approximately 2 µm from cross sectional SEM images of ZnO nanowires grown on silicon. The EDX spectrum shown in Figure 3(d) shows three significant peaks, labelled as carbon, zinc and oxygen. The carbon peak was attributed to the underlying carbon ink electrode and polyimide substrate. The zinc and oxygen peaks were attributed to the ZnO nanowires. Compositional analysis from the spectrum revealed the stoichiometry between zinc and oxygen was close to 1:1

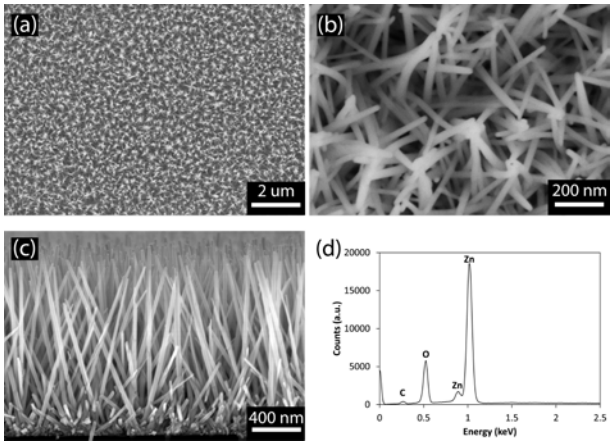

Figure 3: SEM images (a) grown ZnO nanowires on carbon electrode 10 k magnification, (b) grown ZnO nanowires on carbon electrode with 100 k magnification, (c) cross-sectional image of ZnO nanowires and (d) EDX spectrum of the carbon working electrode with ZnO nanowires.

XRD analysis of the ZnO nanowires within the printed seed layer region on the carbon working electrode is shown in Figure 4. From the graph, five significant peaks can be observed. The carbon (111) and AgCl (200) peaks were attributed to the carbon and Ag/AgCl electrodes respectively. A sharp diffraction peak of ZnO associated with (002) crystal plane can be seen in the graph along with additional peaks associated with the ZnO (100) and (101) crystal planes. The large intensity of the ZnO (002) peak as compared to the ZnO (100) and (101) peaks indicates that the ZnO preferentially grown along the c-axis direction as expected.

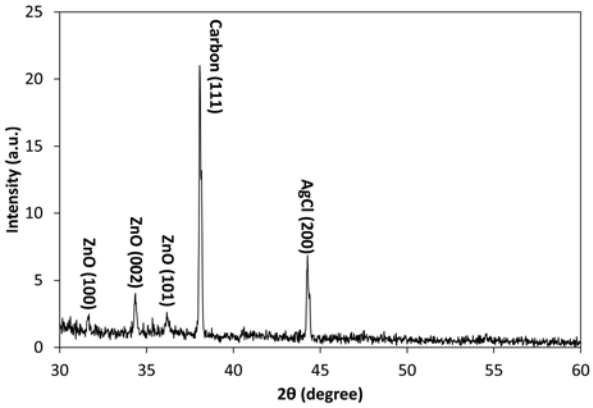

Figure 4: XRD spectrum of the carbon working electrode region with ZnO nanowires.

The stability of the electrochemical biosensor would depend on the stability of the printed reference electrode. Its stability over time is one of the crucial factors for continuous measurement. Here, a commercially available Ag/AgCl screen printing ink was printed on to the polyimide substrate using the flexographic printer without modification to the ink. In the fabrication of the sensors, the devices were floated on an aqueous growth solution at elevated temperature during the hydrothermal growth of the ZnO nanowires. The stability of the printed Ag/AgCl reference electrode could be degraded during the nanowire growth process. In order to investigate this, the stability of the printed Ag/AgCl electrode was evaluated after the hydrothermal growth process and the result is shown in Figure 5(a). For comparison, a printed Ag/AgCl electrode prior to the growth process was also evaluated and the result is shown in Figure 5(b). The drift in open circuit potential over a 72 hour period for the printed Ag/AgCl electrode were 4.6 mV and 3.4 mV for samples before and after the growth process respectively. These values were small compared to the applied potential of 0.8 V and suggested the hydrothermal growth did not have a significant effect on the performance of the reference electrode in terms of the overall long-term stability. However, random

small potential fluctuations can be observed in Figure 5(a). The magnitude of the fluctuations was also relatively small at approximately 2 mV peak. These fluctuations were deemed insignificant to the sensor response but could add to noise levels of the device reducing the limit of detection. The glucose measurements reported in the following section show current traces were relatively smooth over time and only fluctuate upon addition of glucose. This indicated that the reference electrode was not adding any significant noise to the sensor output and was therefore sufficiently stable for the application even after the hydrothermal growth process.

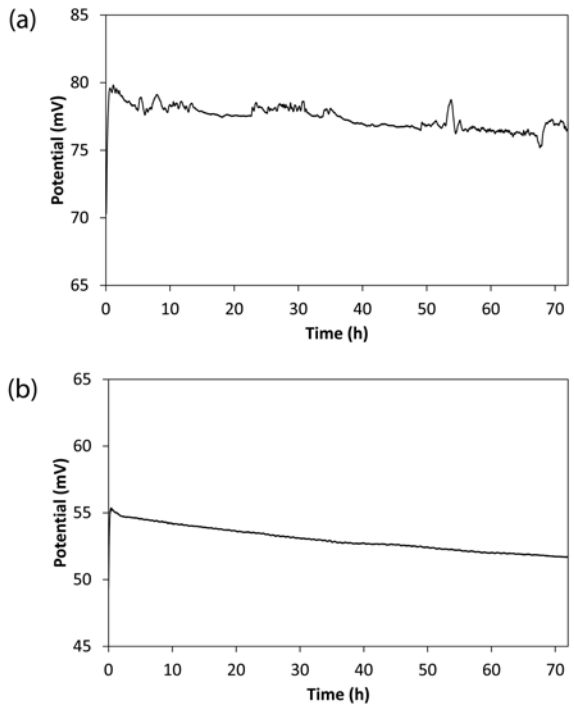

Figure 5: Stability test of printed Ag/AgCl electrode vs. commercial reference electrode (a) after hydrothermal growth and (b) without hydrothermal growth.

3.2 Glucose sensing properties

The nanowire sensor devices were functionalized with GOx for glucose detection as an example of enzymatic sensing with the device. In order to investigate the optimum potential for the glucose detection, the nanowire sensors were characterized using cyclic voltammetry. The potential was swept from 0 V to 0.8 V with a scan rate of 250 mV/s. Figure 6(a) displays the cyclic voltammograms of the sensor. The cyclic voltammetry was performed in unstirred PBS solution with increasing glucose concentrations from 0 mM to 3 mM in 1mM steps. With the addition of glucose in the PBS, a rise in the oxidation current was observed and the maximum rise of oxidation current with

glucose addition was at 0.8 V. This potential was consistent with previous glucose sensors constructed using ZnO nanostructures [34]. The current versus concentration curve displayed in Figure 6(b) shows the nanowire sensor exhibited a linear response to glucose concentration with a correlation coefficient of 0.993 under cyclic voltammetry.

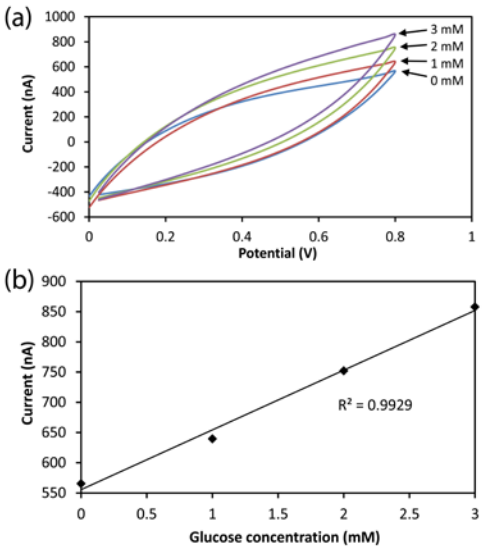

Figure 6: (a) Cyclic voltammograms of printed glucose sensor in PBS solution from 0 mM up to 3 mM glucose concentration and (b) a calibration curve for the response current vs. glucose concentration of the printed glucose sensor at 0.8V.

The continuous glucose sensing properties of the nanowire sensor was investigated via chronoamperometry in PBS solution at an applied potential of 0.8 V under constant stirring. A typical chronoamperometric plot is shown in Figure 7(a), which consisted of a current versus time graph. During the collection of the chronoamperometric data, incremental steps in glucose concentration were made by adding glucose to the PBS solution. Glucose concentration increments of 0.1 mM were made at regular intervals. The sensor could be seen to respond quickly to the addition of glucose into the test solution. The sensors reached 90% of their response within 5 to 10 seconds and showed a relatively stable response between additions. From the chronoamperometric plot, a calibration curve was generated by plotting the steady state current at each concentration against that concentration. The calibration curve for a typical nanowire glucose sensor is shown in Figure 7(b) where the sensor exhibited a linear response to glucose concentration from 0 mM to 1.7 mM with a correlation coefficient of 0.996. The gradient of the calibration curves in the linear region and the area of the working electrodes yield the sensitivity of the sensors. The typical sensitivity of

four separately fabricated nanowire glucose sensors was 1.2 ± 0.2 µA mM^{-1} cm^{-2}. These results indicated that the sensor responded effectively to glucose addition with a calculated limit of detection of 46 ± 31 µM and saturation point of 3.6 ± 0.6 mM. The limit of detection was calculated as the concentration where the current response of the sensors would be three times the peak to peak noise levels in the data. Both the sensitivity and detection limit of the nanowire glucose sensors were in the same order of magnitude as compared to the AuNPs glucose sensors fabricated using similar printing technique on the working electrode only [27]. This demonstrated that the printed Ag/AgCl reference electrode exhibited good stability and did not affect the performance of the sensor.

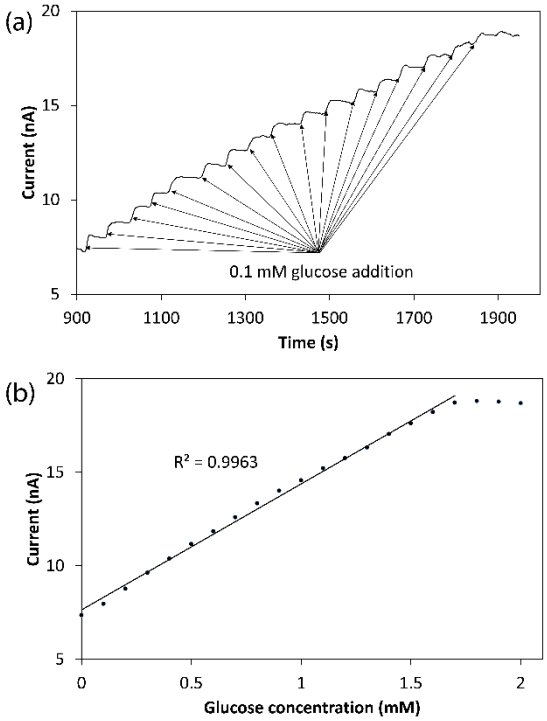

Figure 7: Typical response of printed sensor with chronoamperametry (a) chronoamperametric response with successive addition of glucose with an applied voltage of +0.8V and (b) a calibration curve for the response current versus glucose concentration.

4. Conclusion

Roll-to-roll flexographic printing, which is suitable for low-cost high-volume production, was successfully applied in the fabrication of a three electrode electrochemical biosensor platform incorporating ZnO nanowires. The selective growth of ZnO nanowires on the porous carbon working electrode was performed via patterning of the precursor using the printing technique. This circumvented the need for expensive cleanroom facilities in the

fabrication of nanowire electrochemical biosensing devices. The printed Ag/AgCl reference electrode fabricated onto the sensor exhibited good stability and the typical sensitivity of the nanowire devices in the detection of glucose was 1.2 ± 0.2 μA cm^{-2} mM^{-1}. This is an exemplar sensor, as the device can be modified for other biosensing applications by applying suitable surface functionalization on the nanowires.

Acknowledgement

This work was funded by the Welsh Government (grant no. HE09COL1035).

References

[1] K.V. V Gurav, M.G.G. Gang, S.W.W. Shin, U.M.M. Patil, P.R.R. Deshmukh, G.L.L. Agawane, M.P.P. Suryawanshi, S.M.M. Pawar, P.S.S. Patil, C.D.D. Lokhande, J.H.H. Kim, Sensors Actuators B Chem. 190 (2014) 439–445.

[2] A. Sivapunniyam, N. Wiromrat, M.T.Z. Myint, J. Dutta, Sensors Actuators B Chem. 157 (2011) 232–239.

[3] Y. Wei, Y. Li, X. Liu, Y. Xian, G. Shi, L. Jin, Biosens. Bioelectron. 26 (2010) 275–278.

[4] M.H. Asif, S.M.U. Ali, O. Nur, M. Willander, C. Brännmark, P. Strålfors, U.H. Englund, F. Elinder, B. Danielsson, Biosens. Bioelectron. 25 (2010) 2205–2211.

[5] Q. Ma, K. Nakazato, Biosens. Bioelectron. 51 (2014) 362–5.

[6] Y.T. Wang, Y.J. Bao, L. Lou, J.J. Li, W.J. Du, Z.Q. Zhu, H. Peng, J.Z. Zhu, 2010 IEEE Sensors (2010) 33–37.

[7] R. Niepelt, U.C. Schröder, J. Sommerfeld, I. Slowik, B. Rudolph, R. Möller, B. Seise, A. Csaki, W. Fritzsche, C. Ronning, Nanoscale Res. Lett. 6 (2011) 511.

[8] S.M. Usman Ali, O. Nur, M. Willander, B. Danielsson, Sensors Actuators B Chem. 145 (2010) 869–874.

[9] K. Ogata, H. Dobashi, K. Koike, S. Sasa, M. Inoue, M. Yano, Phys. E Low-Dimensional Syst. Nanostructures 42 (2010) 2880–2883.

[10] J.X. Wang, X.W. Sun, a. Wei, Y. Lei, X.P. Cai, C.M. Li, Z.L. Dong, Appl. Phys. Lett. 88 (2006) 233106.

[11] D. Pradhan, F. Niroui, K.T. Leung, ACS Appl. Mater. Interfaces 2 (2010) 2409–12.

[12] J. Weber, S. Jeedigunta, A. Kumar, J. Nanomater. 2008 (2008) 1–5.

[13] J. Zang, C.M. Li, X. Cui, J. Wang, X. Sun, H. Dong, C.Q. Sun, M. Li, Q. Sun, Electroanalysis 19 (2007) 1008–1014.

[14] S.M.U. Ali, Z.H. Ibupoto, S. Salman, O. Nur, M. Willander, B. Danielsson, Sens. Actuators, B 160 (2011) 637–643.

[15] M. Jacobs, S. Muthukumar, A. Panneer Selvam, J. Engel Craven, S. Prasad, Biosens. Bioelectron. 55 (2014) 7–13.

[16] Y. Zhang, K. Yu, S. Ouyang, Z. Zhu, Phys. B Condens. Matter 382 (2006) 76–80.

[17] Y. Zhang, K. Yu, S. Ouyang, Z. Zhu, Mater. Lett. 60 (2006) 522–526.

[18] Y. Huang, K. Yu, Z. Zhu, Curr. Appl. Phys. 7 (2007) 702–706.

[19] Y. Hu, X. Yan, Y. Gu, X. Chen, Z. Bai, Z. Kang, Appl. Surf. Sci. 339 (2015) 122–127.

[20] C. Chevalier-César, K. Nomenyo, A. Rumyantseva, A. Gokarna, A. Gwiazda, G. Lérondel, Adv. Funct. Mater. (2016) 1787–1792.

[21] J.-C. Chou, Y.-L. Tsai, T.-Y. Cheng, Y.-H. Liao, G.-C. Ye, S.-Y. Yang, IEEE Sens. J. 14 (2014) 178–183.

[22] R. Kitsomboonloha, S. Baruah, M.T.Z. Myint, V. Subramanian, J. Dutta, J. Cryst. Growth 311 (2009) 2352–2358.

[23] Y.N. Liang, B.K. Lok, X. Hu, 2009 11th Electron. Packag. Technol. Conf. (2009) 174–179.

[24] H. Kempa, M. Hambsch, K. Reuter, M. Stanel, G.C. Schmidt, B. Meier, A.C. Hübler, IEEE Trans. Electron Devices 58 (2011) 2765–2769.

[25] T. Fischer, N. Wetzold, L. Kroll, A. Hübler, A. Hu, J. Appl. Polym. Sci. 129 (2013) 2112–2120.

[26] J. Baker, D. Deganello, D.T. Gethin, T.M. Watson, Mater. Res. Innov. 18 (2014) 86–90.

[27] J. Benson, C.M. Fung, J.S. Lloyd, D. Deganello, N.A. Smith, K.S. Teng, Nanoscale Res. Lett. 10 (2015) 1–8.

[28] J.S. Lloyd, C.M. Fung, D. Deganello, R.J. Wang, T.G.G. Maffeis, S.P. Lau, K.S. Teng, Nanotechnology 24 (2013) 195602.

[29] A.K. Assaifan, J.S. Lloyd, S. Samavat, D. Deganello, R.J. Stanton, K.S. Teng, ACS Appl. Mater. Interfaces 8 (2016) 33802–33810.

[30] T. V. Plakhova, M. V. Shestakov, A.N. Baranov, Inorg. Mater. 48 (2012) 469–475.

[31] K.A. Wahid, W.Y. Lee, H.W. Lee, A.S. Teh, D.C.S.S. Bien, I.A. Azid, K. Anuar, W. Yee, H. Wah, A. Shin, I. Abd, Appl. Surf. Sci. 283 (2013) 629–635.

[32] J.S. Lloyd, C.M. Fung, E.J. Alvim, D. Deganello, K.S. Teng, Nanotechnology 26 (2015) 265303.

[33] M.C. Akgun, Y.E. Kalay, H.E. Unalan, J. Mater. Res. 27 (2012) 1445–1451.

[34] Z.W. Zhao, X.J. Chen, B.K. Tay, J.S. Chen, Z.J. Han, K. a Khor, Biosens. Bioelectron. 23 (2007) 135–9.